Lattice dynamics of the model percolation-type (Zn,Be)Se alloy: Inelastic neutron scattering, *ab initio* study, and shell-model calculations

Mala N. Rao,[1] D. Lamago,[2] A. Ivanov,[3] M. d'Astuto,[4] A. V. Postnikov,[5] R. Hajj Hussein,[5] Tista Basak,[1] S. L. Chaplot,[1] F. Firszt,[6] W. Paszkowicz,[7] S. K. Deb,[8] and O. Pagès[5,*]

[1]*Solid State Physics Division, Bhabha Atomic Research Centre, Mumbai 400085, India*
[2]*Laboratoire Léon Brillouin, CEA-CNRS Saclay, 91191 Gif-Sur-Yvette, France*
[3]*Institut Laue Langevin, 6 rue Jules Horowitz, 38042 Grenoble Cedex 9, France*
[4]*Institut de Minéralogie et de Physique des Milieux Condensés, CNRS, Université Paris 6, France*
[5]*Université de Lorraine, LCP-A2MC, Institut Jean Barriol, Metz 57078, France*
[6]*Institute of Physics, N. Copernicus University, 87-100 Toruń, Poland*
[7]*Institute of Physics, Polish Academy of Sciences, 02-668 Warsaw, Poland*
[8]*Raja Ramanna Centre for Advanced Technology, Indore 452013, India*
(Received 23 November 2012; revised manuscript received 3 March 2014; published 7 April 2014)

The random $Zn_{1-x}Be_xSe$ zincblende alloy is known to exhibit a peculiar three-mode [$1\times$ (Zn-Se),$2\times$ (Be-Se)] vibration pattern near the Brillouin zone (BZ) center, of the so-called percolation type, apparent in its Raman spectra. This is due to an unusually large contrast between the physical properties (length, ionicity) of the constituting bonds. In the present work, the inelastic neutron scattering is applied to study the dispersion of modes away from the BZ center, with special attention to the $\vec{q}$ dependence of the BeSe-like transverse optic doublet. The discussion is supported by calculations of lattice dynamics done both *ab initio* (using the SIESTA code) and within the shell model. The BeSe-like doublet is found to survive nearly unchanged throughout the BZ up to the zone edge, indicating that its origin is at the ultimate bond scale. The microscopic mechanism of splitting is clarified by *ab initio* calculations. Namely, the local lattice relaxation needed to accommodate the contrast in physical properties of the Zn-Se and Be-Se bonds splits the stretching and bending modes of connected, i.e., percolativelike, (Be-Se) bonds.

I. INTRODUCTION

Alloying is traditionally appealing because it allows one to tune various properties by concentration in large limits [1]. In this work we are specifically interested in the vibration properties of $A_{1-x}B_xC$ zincblende semiconductor alloys [also noted $(A,B)C$, C referring independently to the cationic or to the anionic species], which have attracted considerable attention both experimentally and theoretically since the emergence of such systems in the mid-sixties [2]. Most experimental data were obtained by using optical techniques such as Raman scattering (in a conventional backscattering setup) or infrared absorption. Due to the quasivertical dispersion of light at the scale of the Brillouin zone (BZ), these techniques detect only optic phonons near the center of the BZ ($q \approx 0$, Γ), staying, at most, within a few percent of the BZ size.

Such Γ-like optic modes correspond to a relative displacement of the intercalated C-only and (A,B)-mixed fcc sublattices, both considered to be quasirigid ones. We focus on the transverse optic (TO) modes, referring to atom displacements perpendicular to the direction of propagation. This is because the detected TO modes in the traditional Raman and infrared spectra consist of purely mechanical vibrations, and, as such, hardly couple. They are thus well suited for revealing the intrinsic phonon pattern due to a given bond in a complex system like an alloy [2]. In contrast, the longitudinal optic (LO) modes couple via their macroscopic electric field due to the ionicity of the chemical bonding in such

a polar crystal as a zincblende alloy. This usually leaves the misleading impression of an over simple phonon pattern [3]. On the theoretical side, it is important to note that near Γ, the space phase term $(\vec{q} \cdot \vec{r})$ in the description of an optic phonon disappears and, along with it, all information on the actual position $(\vec{r})$ of an atom in the three-dimensional crystal. This justifies a simple one-dimensional discussion of the optic modes near Γ, in the spirit of a linear-chain approximation in which the bond bending is by construction omitted, which has resulted in the emergence of meaningful phenomenological models, as discussed below [2,3].

In this work, our aim is to extend the study of the vibration properties of a particular zincblende alloy, namely $Zn_{1-x}Be_xSe$, outside Γ and over the whole BZ by using inelastic neutron scattering (INS). (Zn,Be)Se is interesting for such extended vibrational study since its detailed Raman analysis over the past decade has revealed an atypical TO bimodal pattern in the spectral range of the short Be-Se bond, already near Γ [3]. This was attributed to an unusually large contrast between the bond physical properties (length, ionicity) of its constituent species (Zn-Se and Be-Se), detailed at a later stage. The point is that the Be-Se bimodal Raman pattern of (Zn,Be)Se could not be explained within the known phenomenological models operating near Γ, namely the modified-random-element-isodisplacement (MREI) model of Chang and Mitra [4] and the alternative cluster model developed by Verleur and Barker [5] corresponding to a 1-bond → 1-TO behavior and a 1-bond → 4-TO one, respectively. To this end, the phenomenological *percolation model*, corresponding to a 1-bond → 2-TO behavior, has been developed [3]. Details concerning the MREI, cluster, and percolation schemes are

---

*Corresponding author: olivier.pages@univ-lorraine.fr

reported in a dedicated section (see Sec. III). We retain that, retrospectively, the percolation model seems to be universally applicable to zincblende alloys, and even to allow extension to diamond-structure alloys [6], eliminating the need to resort to *ad hoc* subtypes of the previous MREI and cluster models.

The percolation-type frequency gap Δ between two "like" TO modes due to the same bond of a given $(A,B)C$ zincblende alloy, more precisely denoted $\Delta_{A\text{-}C}$ or $\Delta_{B\text{-}C}$ depending on the considered bond, summarizes the essence of the 1-bond $\rightarrow$ 2-TO percolation behavior. It is thus essential to clarify the physics behind such parameter. The central issue is whether Δ survives, or not, away from Γ, namely at finite wavelengths, and if so down to which length scale? This might help identify the microscopic origin of splitting. We hope that a direct insight will be achieved by INS in this work.

Experimentally, (Zn,Be)Se is an ideal case for INS due to its sensitivity for the detection of light elements, like Be, in a heavy elements matrix, like ZnSe. The analysis focuses on the sensitive Be content of 33 at.%, corresponding to the best compromise in terms of relative intensities of the $\text{TO}^{\text{Be}}_{\text{Be-Se}}$ and $\text{TO}^{\text{Zn}}_{\text{Be-Se}}$ Raman modes (refer to the f terms in Sec. III) and also of the magnitude of the percolation-type frequency gap $\Delta_{\text{Be-Se}}$ that separates them (a Raman insight is given below).

More generally, we are not aware of any INS study of the phonon dispersion in a $(A,B)C$ zincblende alloy in the literature. INS measurements have been done on zincblende magnetic alloys, but the attention there was focused on magnons rather than on phonons [7]. Nevertheless, the question has motivated theoretical works [8,9]. The main theoretical trends are summarized hereafter.

Technically, for $q \neq 0$, i.e., away from Γ, the information on the position of an atom reappears in the phase of a phonon, which forces us to adopt a realistic description of the crystal in three dimensions and thus to consider both central (bond-stretching) and noncentral (bond-bending) interatomic forces. One crucial issue remains as how to describe the $A \leftrightarrow B$ substitutional disorder.

One may use some mean-field approximation, e.g., the virtual crystal approximation. A generalized MREI approach was developed in that spirit by Varshney *et al.* [8] and applied to the disordered $\text{ZnS}_{0.5}\text{Se}_{0.5}$ and $\text{GaAs}_{0.5}\text{P}_{0.5}$ alloys. The model has predicted a basic 1-bond $\rightarrow$ 1-TO MREI-like pattern for the $\text{ZnS}_{0.5}\text{Se}_{0.5}$ and $\text{GaAs}_{0.5}\text{P}_{0.5}$ optic phonons, plus a mixed 2-bond $\rightarrow$ 1-mode type for the acoustic ones [10], throughout the BZ.

More realistic phonon calculations may come about when applying standard lattice dynamics techniques using fully relaxed supercells. One may proceed either *ab initio* or by using force constants derived from a certain ion-to-ion interaction potential. We are aware of only one such earlier work, namely the *ab initio* study of the disordered $\text{Al}_{0.5}\text{Ga}_{0.5}\text{As}$ alloy by Baroni *et al.* [9]. In the cited work, the natural contrast in the Al-As and Ga-As bond-stretching and bond-bending force constants, identified as one source of lattice distortion, was neglected. The difference between the two Al and Ga cations was taken into account only through their masses. As the difference in bond length, i.e., another source of lattice distortion, is already negligible ($\sim 0.1\%$) in this alloy [11,12], the above approximation on the bond force constants comes, in practice, to consider a quasiregular lattice for disordered $\text{Al}_{0.5}\text{Ga}_{0.5}\text{As}$, as if this were a pure binary compound. The as-calculated dispersion of optic phonons for $\text{Al}_{0.5}\text{Ga}_{0.5}\text{As}$ was found to obey a 1-bond $\rightarrow$ 1-mode MREI-like behavior both in Γ and throughout the BZ (see Fig. 3 of Ref. [9]).

Note that the $\text{ZnS}_{0.5}\text{Se}_{0.5}$, $\text{GaAs}_{0.5}\text{P}_{0.5}$, and $\text{Al}_{0.5}\text{Ga}_{0.5}\text{As}$ alloys discussed above are characterized by relative mild contrasts in bond length ($\sim 4\%$, $\sim 4\%$, and $\sim 1\%$, correspondingly) and in bond ionicity ($\sim 3\%$, $\sim 3\%$, and $\sim 15\%$) [11,12]. The corresponding contrasts are much larger in (Zn,Be)Se, at least by a factor three, as detailed at a later stage. We thus expect that the latter alloy will provide a refined insight into the lattice dynamics of a $(A,B)C$ zincblende alloy away from Γ beyond the $[1 \times (A\text{-}C), 1 \times (B\text{-}C)]$ two-mode MREI-like approximation that is valid for the above systems. We already know, as discussed above, that (Zn,Be)Se yields a more complicated vibration pattern than the MREI-like one in Γ.

The manuscript is organized as follows. In Sec. II we give details concerning the sample preparation (Sec. IIA), the Raman and INS experiments (Sec. IIB), and related calculations of the (Zn,Be)Se lattice dynamics using the *ab initio* SIESTA code and the shell model (Sec. IIC). In Sec. III we introduce the basic contents of the phenomenological MREI, cluster, and percolation models used for the discussion of the lattice dynamics of a zincblende alloy near Γ for reference purposes. The experimental results obtained with (Zn,Be)Se, discussed in the light of calculations, are reported in Sec. IV. Section IVA provides a reference Raman (Sec. IVA1)/*ab initio* (Sec. IVA2) insight into the optic phonons of (Zn,Be)Se near Γ. This is useful both to decide about the nature (random vs nonrandom) of the $\text{Zn} \leftrightarrow \text{Be}$ substitution in the $\text{Zn}_{0.67}\text{Be}_{0.33}\text{Se}$ sample studied by INS (Sec. IVA1) and further to elucidate the microscopic mechanism at the origin of $\Delta_{\text{Be-Se}}$ in the Be-dilute limit (Sec. IVA2). Section IVB reports on a combined experimental (INS) and theoretical (lattice dynamics calculations, either done *ab initio* or within the shell model) study of the vibration properties of $\text{Zn}_{0.67}\text{Be}_{0.33}\text{Se}$ away from Γ. In Sec. IVB1, the simulation of what can be expected for the $\vec{q}$-dependent densities of modes away from Γ is outlined on the basis of *ab initio* calculations using large $\text{Zn}_{0.67}\text{Be}_{0.33}\text{Se}$ supercells, with special attention to $\Delta_{\text{Be-Se}}$. The actual INS measurements, done with the $\text{Zn}_{0.67}\text{Be}_{0.33}\text{Se}$ alloy and directly discussed in light of the shell model, are reported in Sec. IVB2. Concluding remarks are summarized in Sec. V.

II. EXPERIMENTAL DETAILS AND CALCULATION METHODS

A. Samples

Two $\text{Zn}_{0.67}\text{Be}_{0.33}\text{Se}$ samples were grown from the melt by using the high-pressure Bridgman method. Extensive details concerning the growth technique are available, e.g., in Refs. [13,14]. The ZnSe 6 N Koch-Light and Be (purity $> 99\%$) powders were mixed in stoichiometric proportion and put into a graphite crucible. The crucible was kept at 1830 K for 14 h and then moved out from the heating zone at a speed of 2.4 mm/h. An argon overpressure of 12 MPa was maintained during the growth process. X-ray investigations show that the samples exhibit a single sphalerite

(zincblende) phase. We have discussed elsewhere that the Zn ↔ Be substitution can be considered as random in such crystals grown from the melt within the composition domain 10-54 at.% Be [15]. However, a specific analysis of the Zn ↔ Be substitution for the samples used in this work is developed below.

The first sample was ground into a fine powder and used for INS measurement of the (Zn,Be)Se one-phonon density of states (Ph-DOS). The second sample was prepared as a large size single crystal (cylinder, ∼8 mm in diameter, ∼20 mm in length) cut perpendicular to its [110]-growth direction and then mechanically polished to optical quality. The latter single crystal receives most of our attention in this work, being studied both by Raman scattering and by INS. In particular, it is used to explore the phonon dispersion of (Zn,Be)Se along the usual high-symmetry [001], [110], and [111] directions of the BZ. Neutron diffraction was used to establish the single crystallinity of the cylindrical ingot and to identify its growth direction, as specified above, and further to establish the single-phase character of the polycrystalline grains constituting the powder.

An additional ∼1-μm-thick fully relaxed $Zn_{0.69}Be_{0.31}Se$ layer, deposited by molecular beam epitaxy onto a (001)-oriented GaAs substrate (see Ref. [3] and references therein), was used to access the LO Raman mode of (Zn,Be)Se, which cannot be recorded when using the single crystal (see detail below).

For each sample, the Be content was determined with a typical accuracy of ±0.5% from the lattice constant measured by x-ray diffraction assuming Vegard's rule.

B. Raman and INS experiments

In a standard backscattering Raman experiment along the [110]-growth axis of the $Zn_{0.67}Be_{0.33}Se$ ingot, in principle, only the TO mode is allowed; however, a reminiscence of the LO mode, theoretically forbidden, showed up almost as strongly as the allowed TO modes. A pure-TO Raman insight could nevertheless be achieved in the cross-polarization mode of the incident and scattered beams and rotating the sample around its [110]-growth axis. In such geometry, quoted for further reference as geometry 1, the intensities of both the allowed TO modes and of the theoretically forbidden LO modes decrease but at a faster rate for the LO mode than that for the TOs, so that at a certain stage only the TO modes survived. A pure-LO insight around 30 at.% Be was obtained by analyzing the (001)-oriented $Zn_{0.69}Be_{0.31}Se$ epitaxial layer in a backscattering geometry along its [001]-growth axis, henceforth referred to as geometry 2 [3]. A pure-TO Raman spectrum was also taken from the epilayer in backscattering geometry along its [110]-edge axis, referred to as geometry 1' [3].

The Raman microprobe was used because high spatial resolution was needed in geometry 1'. The pure-TO (geometry 1') and pure-LO (geometry 2) Raman spectra of the epilayer were taken by using the nonresonant 514.5-nm Ar+ laser line. For recording the pure-TO Raman spectrum of the (110)-oriented single crystal (in geometry 1), the alternative 633.0 nm He-Ne laser line was preferred, notwithstanding its inferior Raman efficiency. Note that the perfect LO extinction

ideally expected in geometry 1 could be achieved only with the latter laser line. Otherwise a residual LO mode was systematically detected [refer, e.g., to the top spectrum of Fig. 2(a) in Ref. [16], taken with the 514.5-nm Ar+ excitation]. A typical laser output of 10 mW was used for both excitations, corresponding to a standard illumination of ∼1 MW/cm^2 for a ∼1-μm laser spot onto the sample surface.

INS experiments were carried out at the IN1 spectrometer of the Institut Laue–Langevin in Grenoble and at the thermal neutron spectrometer 1T1 of the Laboratoire Leon Brillouin in Saclay. The sample was placed in a closed-cycle cryostat and held at 13 K in both cases. The IN1 neutron spectrometer, operated in the Be filter mode, was used to measure the Ph-DOS of the $Zn_{0.67}Be_{0.33}Se$ powder with both Cu200 and Cu220 monochromators. The measured spectrum was normalized to the counts of a monitor detector mounted before the sample, thus accounting for changes in the incident neutron flux. A spectrum of the aluminum foil holding the sample was taken separately, yielding a background measurement. The 1T1 neutron spectrometer was used to probe different $\vec{q}$ points in reciprocal space along the [100], [110], and [111] high-symmetry directions of the BZ of the $Zn_{0.67}Be_{0.33}Se$ single crystal covering the Zn-Se (with fixed final energy 14.7 meV) and Be-Se (with fixed final energy 34.8 meV) spectral ranges in both the transverse and longitudinal symmetries in the constant-momentum transfer mode of operation. Only energy loss was considered.

C. Lattice dynamics calculations

For line profile modeling of the experimental Raman lineshapes, we use the following generic expression of the multimode Raman cross section (RCS), as derived within the formalism of the linear dielectric response developed by Hon and Faust [17], using scalar equations of motion (justified by the $q \sim 0$ approximation, as explained in Sec. III) [3],

$$RCS(\omega,x) \propto Im\left\{-\frac{1}{\varepsilon_r(\omega,x)} \times \left[1 + \sum_p C_p(x) \times L_p(\omega,x)\right]^2 \right.$$
$$\left. + \sum_p \frac{C_p^2(x) \times \omega_p^2(x) \times L_p(\omega,x)}{S_p(x) \times \varepsilon_{\infty,p} \times \omega_p^2}\right\}. \quad (1)$$

$\varepsilon_r(\omega,x)$ is the relative dielectric function of the (Zn,Be)Se alloy, taken in the classical form $\varepsilon_{\inf.}(x) + \sum_p \varepsilon_{\infty,p} \times S_p(x) \times L_p(\omega,x_p)$. While $\varepsilon_r(\omega,x)$ diverges for a TO mode, it vanishes for a LO mode, so that the TO and LO RCSs are governed by the second and first terms of Eq. (1), respectively. The summation runs over all possible ionic oscillators, i.e., three in total our $[1 \times (Zn - Se), 2 \times (Be - Se)]$ percolation-type description ($p = 1-3$), while $\varepsilon_{\inf.}(x)$ is a linear x-dependent form of the electronic contribution. Each TO resonance at frequency $\omega_p(x)$ is modeled by using a Lorentzian profile $L_p(\omega,x) = \omega_p^2(x) \times (\omega_p^2(x) - \omega^2 - j \times \gamma_p(x) \times \omega)^{-1}$, with damping parameter $\gamma_p(x)$. $S_p(x)$ and $C_p(x)$ are the oscillator strength and Faust-Henry coefficient related to oscillator p, respectively. Both scale linearly with the fraction of that oscillator in the crystal. Alternative input parameters are the ZnSe and BeSe $(S_p, C_p, \omega_p, \varepsilon_{\inf,p})$ parent values, corresponding to
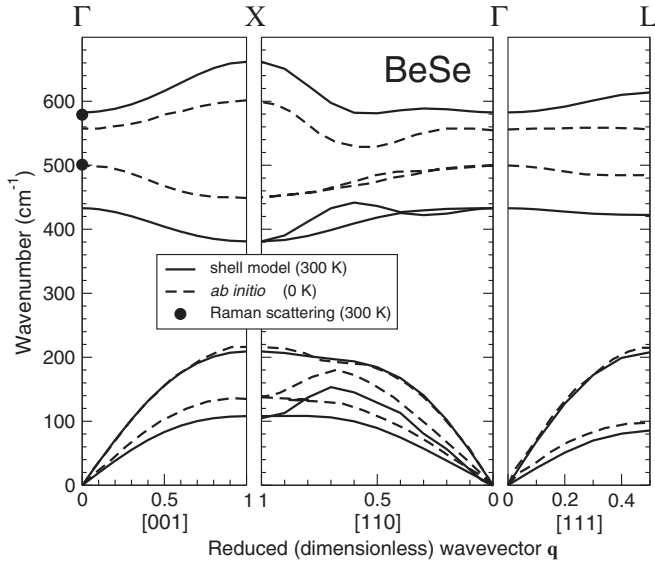
FIG. 1. BeSe phonon dispersion calculated at 300 K within the shell model (solid lines). The corresponding *ab initio* curves at 0 K taken from Ref. [24] (dashed lines) and the Raman frequencies measured at 300 K (near Γ, thick dots) taken from Ref. [23] are added for comparison.

$(2.92, -0.7, 254.5 \text{ cm}^{-1}, 5.75)$ and $(1.77, -0.7, 468.5 \text{ cm}^{-1}, 5.32)$, respectively [3].

The best $\vec{q}$ points at which the INS measurements should be carried out are selected from dynamical structure factor computations done at 0 K by applying a shell model to a series of 20 different $\text{Zn}_{21}\text{Be}_{11}\text{Se}_{32}$ (64-atom) $2 \times 2 \times 2$ supercells ($\sim$33 at.% Be) in which the Zn and Be atoms are distributed at random, with averaging over all 20 configurations at the end. It was confirmed that in each supercell the counting of the five possible Se-centered tetrahedral units (with numbers of Be atoms at the corners varying from 0 to 4) more or less matched the theoretical statistics in case of a random $\text{Zn} \leftrightarrow \text{Be}$ substitution, as established, e.g., along the cluster model developed by Verleur and Barker (refer to the f_i terms in Eqs. (5)–(9) of Ref. [5], taking parameter $\beta = 0$).

The atoms are modeled by using the shell model, as described in Ref. [18]. The input parameters of the shell model were adjusted from physical observables related to the pure ZnSe and BeSe parent compounds, including the bulk modulus [19], the lattice constant [20], and the TO and LO Raman frequencies [21]. The phonon dispersion curves calculated for the pure ZnSe and BeSe compounds along the usual high-symmetry directions in reciprocal space within the shell model (the procedure is detailed below) are shown in Ref. [22] and in Fig. 1, respectively. Note that for each compound, the magnitude of the TO-LO splitting predicted by the shell model is roughly doubled with respect to the experimental (Ref. [23]) and/or *ab initio* (Ref. [24]; see Fig. 1 therein) references throughout the whole BZ. Besides, the transverse acoustical frequencies are generally underestimated for BeSe (see Fig. 1), whereas they appear to be slightly overestimated in the case of ZnSe (Ref. [22]). Otherwise, the theoretical phonon dispersion curves given by the shell model reproduce rather well the general pattern existing in the

ZnSe [22] and BeSe (see Fig. 1) experimental and/or *ab initio* curves in the literature.

Regarding the alloy, we proceed as follows. After full relaxation (atom coordinates and lattice constant) of a given 64-atom supercell, a diagonalization of the dynamical matrix obtained by employing the above potential in the shell-model equations of motion yields frequencies and eigenvectors of all 192 (64×3) vibrational modes at a given $\vec{q}$ point. By repeating the procedure for a series of $\vec{q}$ points taken along a given direction in reciprocal space, one obtains a theoretical insight into the phonon dispersion along that direction in both the transverse and longitudinal symmetries (depending on whether the atom displacement is perpendicular to the considered direction in reciprocal space or along that direction, respectively). Subsequent reduction of all the branches present in a supercell to the branches actually present for the underlying unit cell is done by analyzing the neutron scattering cross-section. This gives finite values for the real branches, while it is nearly zero for the folded branches. The $\vec{q}$-dependent (one-phonon inelastic) neutron scattering cross section is eventually given by the following equation:

$$S(\vec{Q}, \omega) = A \sum_{qj} \frac{\hbar}{2\omega(qj)} [n(\omega) + \tfrac{1}{2} \mp \tfrac{1}{2}] \left| F_j^{(1)}(\vec{Q}) \right|^2$$

$$\times \delta(\vec{Q} - \vec{G} + \vec{q}) \delta(\omega \mp \omega(qj)), \qquad (2)$$

where

$$F_j^{(1)}(\vec{Q}) = \sum_k b_k^{\text{coh}} \frac{\vec{Q} \cdot \vec{\xi}(qj, k)}{\sqrt{m_k}} \exp[-W_k(\vec{Q})]$$

$$\times \exp[i\vec{G} \cdot \vec{X}(k)], \qquad (3)$$

with b_k^{coh} and m_k referring to the coherent neutron scattering length and to the mass of atom k, respectively. $\vec{X}(k)$ is the coordinate vector, $\exp[-W_k(\vec{Q})]$ is the Debye-Waller factor, and A is a proportionality constant. $\hbar\omega$ and $\hbar\vec{Q}$ are, respectively, the energy transfer and momentum on scattering of the neutron, while $n(\omega)$ is the phonon population factor, given by

$$n(\omega) = [\exp(\omega/k_B T) - 1]^{-1}, \qquad (4)$$

where k_B is the Boltzmann constant. The upper and lower $-$ and $+$ signs in Eq. (2) correspond to energy loss (our experimental case, see above) and energy gain of the neutrons, respectively. The two delta functions stand for the conservation of momentum and energy. The frequencies were coded with respect to their calculated neutron cross-section at each $\vec{q}$ point. This helped in identifying preferential $\vec{q}$ points at which the INS measurements should be performed. The code is also useful to provide a theoretical insight into the phonon dispersion curves of the alloy.

Once the phonon dispersion curves are properly determined via the shell model, the theoretical Ph-DOS immediately follows, given by

$$g(\omega) = N \int_{\text{BZ}} \sum \delta(\omega - \omega_j(\vec{q})) d\vec{q}, \qquad (5)$$

with N as a normalization factor such that $\int g(\omega) d\omega = 1$, being clear that $g(\omega) d\omega$ is the ratio of the number of eigenstates

in the frequency interval $(\omega, \omega + d\omega)$ to the total number of eigenstates. Here, $\omega_j(\vec{q})$ is the phonon frequency of the jth normal mode at wavevector $\vec{q}$.

The discussion of the Raman and INS data, more specifically in reference to the phonon dispersion curves along the [100] direction in reciprocal space ($\Gamma \to X$) in the latter case, is independently supported by *ab initio* calculations at 0 K of the $\vec{q}$-projected transverse and longitudinal Ph-DOS of the phonon BZ of (Zn,Be)Se supercells (see detail below). The calculations are done after full relaxation of the supercells (of the atom positions and of the lattice constant) in the local density approximation by applying the method and computer code SIESTA [25] using the basis functions and pseudopotentials, as explained (including accuracy issues) in Ref. [26]. We emphasize that the *macroscopic* electric field accompanying the LO mode near the center Γ of the BZ is not taken into account in our *ab initio* calculations. The problem disappears immediately away from Γ.

For direct insight into the microscopic origin of the percolation splitting $\Delta_{\text{Be-Se}}$, as apparent in the pure-TO Raman spectra of the (Zn,Be)Se alloy, we calculate the TO DOS projected at the zone center (Γ-projected T–Ph-DOS) of the most simple Be-impurity motif that is likely to produce the observed ($\text{TO}_{\text{Be-Se}}^{\text{Be},1}, \text{TO}_{\text{Be-Se}}^{\text{Zn},1}$) Raman doublet, i.e., merely a pair of connected Be-Se bonds, noted "–Be–Se–Be–" hereafter, inserted in bulk ZnSe [6]. Such atom arrangement is represented by a cubic $2 \times 2 \times 2$ $\text{Be}_2\text{Zn}_{30}\text{Se}_{32}$ (64-atom) supercell. In doing so, we proceed along the frozen phonon technique, following an approach used in Ref. [26]. Specifically, we constructed the density of vibration modes projected onto Γ, related to a particular atom species κ:

$$I_\kappa(\omega, \vec{q} = \vec{0}) = \sum_i \left| \sum_{\alpha \in \kappa} \vec{A}_i^\alpha \right|^2 \delta(\omega - \omega_i), \qquad (6)$$

where α runs over the atoms (in the supercell) of species κ, i numbers the $3\times$ (total number of atoms in supercell) vibration modes, $\vec{A}_i^\alpha$ is an eigenvector of mode, and $\delta(\omega)$ is, optionally, a broadening function, convenient to produce a continuous distribution in place of discrete peaks. In the following figures, the broadening half-width of 2 cm^{-1} is used. Though the matrix elements of Raman scattering are not taken into account in the calculation, the $\Gamma-$projected T–Ph-DOS per Be atom compares directly to the BeSe-like TO Raman signal, in principle, at least regarding the phonon frequencies, if not the Raman intensities.

The reason for focusing on such simple Be-impurity motif as the Be-pair is that the vibration pattern behind the individual features of the Γ-projected T–Ph-DOS per Be atom can be unambiguously deciphered. When using more sophisticated Be-impurity motifs, the percolation splitting $\Delta_{\text{Be-Se}}$ also comes out in the Γ-projected T–Ph-DOS per Be atom, but then the increased complexity of the local lattice relaxation considerably distorts, and eventually obscures, the individual atom displacements, making the assignment of the individual Be vibration modes highly hazardous. We have checked that the 64-atom supercell is well-converged in size and reproduces the Γ-projected T–Ph-DOS per Be atom of the considered –Be–Se–Be– impurity motif as if this is immersed in an infinite ZnSe host matrix.

Ab initio calculations of the longitudinal (superscript L below) and transverse (superscript T) Ph-DOS of $\text{Zn}_{0.67}\text{Be}_{0.33}\text{Se}$ along the $\Gamma \to X$ direction of the reference BZ of the underlying fully relaxed zincblende lattice, in relation to the INS measurements of the phonon dispersion, were then performed, employing a more sophisticated projection scheme than in Eq. (6):

$$I_\kappa^{\text{L}}(\omega, \vec{q}) = \sum_i \left| \sum_{\alpha \in \kappa} \left(\frac{\vec{q}}{|\vec{q}|} \cdot \vec{A}_i^\alpha e^{i\vec{q} \cdot \vec{R}_\alpha} \right) \right|^2 \delta(\omega - \omega_i), \quad (7)$$

$$I_\kappa^{\text{T}}(\omega, \vec{q}) = \sum_i \left| \sum_{\alpha \in \kappa} \left[\vec{A}_i^\alpha - \frac{(\vec{q} \cdot \vec{A}_i^\alpha)}{|\vec{q}|^2} \vec{q} \right] e^{i\vec{q} \cdot \vec{R}_\alpha} \right|^2 \delta(\omega - \omega_i). \tag{8}$$

In addition to the entries explained above, these formulae contain an (arbitrary) $\vec{q}$-vector and the explicit position of the atom α, $\vec{R}_\alpha$. The projections discriminate the Cartesian components of the phonon eigenvector parallel to a given $\vec{q}$ [longitudinal mode, Eq. (7)] and normal to it [transverse mode, Eq. (8)]. We note that the projections are done on the same set of phonon modes; the variation of intensity depending on $\vec{q}$ enhances some modes and suppresses the others, producing, in a large enough supercell, the effect of dispersion with $\vec{q}$.

Because the $\vec{q}$ dispersion is our primary interest for comparison with the INS data, the considered supercells were elongated in the $\Gamma \to X$ direction: the $6 \times 2 \times 2$ replication of an 8-atom cube produced a 192-atom $\text{Zn}_{0.67}\text{Be}_{0.33}\text{Se}$ supercell, on whose cationic sites the Zn and Be atoms are distributed following the technique of special quasirandom supercell construction [27]. The layer-by-layer placement of cations in consecutive (100) planes of the first supercell can be coded by 8-digit binary sequences, with 1 standing for Be and 0 for Zn. Each sequence scans eight cation positions in the 2×2 (y, z) supercell cross-section row by row, e.g., four rows with two sites each. The coding sequences for the 12 (100) planes, expressed as 2-digit hexadecimals, are 7D, 40, 18, 0A, C6, 26, 2A, 25, 00, 48, 03, 6C. Correspondingly, the number of Be atoms in consecutive layers reads $6 + 1 + 2 + 2 + 4 + 3 + 3 + 3 + 0 + 2 + 2 + 4 = 32$ (supercell 1). It is noteworthy that the generated supercell included one Zn-only plane, which might seem somehow "special." The validity of results has been checked by trying another seed, resulting in a different quasirandom supercell, with Be numbers varying from 1 to 5 throughout the (100) layers (supercell 2). The coding of layers reads in this case 40, A4, 28, 42, 73, CA, A2, 89, 18, 2B, 02, 28. The number of Be atoms layer by layer reads $1 + 3 + 2 + 2 + 5 + 4 + 3 + 3 + 2 + 4 + 1 + 2 = 32$. The resulting q_x-dependent T–Ph-DOS per Zn atom and per Be atom are constructed via a projection of the available phonon modes (3×192 total) onto equally spaced q values along $\Gamma \to X$, emphasizing the atom displacements perpendicular to [100] (transverse character) or along [100] (longitudinal character).

III. PHENOMENOLOGICAL CONTEXT NEAR Γ: MREI AND CLUSTER SCHEMES VS PERCOLATION SCHEME

For a better understanding of the proposed INS study of (Zn,Be)Se in this work, we discuss briefly the percolation

scheme in the context of phenomenological models used for the discussion of the Raman and infrared measurements near Γ, focusing on TO modes (see Sec. I). We emphasize, though, that once the composition dependence of both frequency and intensity of the zone-center TO modes of a given zincblende alloy is properly formalized within some appropriate phenomenological model, the LO modes immediately follow from this analysis [2].

Historically, the two phenomenological models used for decades for the theory of the Γ-like TO phonons in $(A,B)C$ zincblende alloys are the MREI [4] and cluster [5] models. In the MREI model, a given A-C or B-C bond is considered to be insensitive to its local environment, thus providing a unique Raman or infrared TO feature at a given alloy composition (1-bond $\rightarrow$ 1-mode scheme). This corresponds to a two-mode (TO$_{A\text{-}C}$, TO$_{B\text{-}C}$) behavior for a random zincblende alloy, the several variants of which are detailed, e.g., in Ref. [4]. When the alloy composition changes, the distinct TO$_{A\text{-}C}$ and TO$_{B\text{-}C}$ modes shift smoothly between their respective bulk and impurity limits, their intensities being scaled as the related bond fractions, i.e., as $1 - x$ and x, respectively. The cluster model was developed for those presumed nonrandom alloys that exhibit more than one TO phonon per bond in their Raman or infrared spectra, such as Ga(As,P) [5]. This model emphasizes an effect on a given bond of its first-neighbor shell in a real three-dimensional crystal, yielding four possible types in a zincblende alloy, hence a generic 1-bond $\rightarrow$ 4-mode TO vibration pattern, corresponding to eight TO modes for a random zincblende alloy. In a frequency vs composition plot, this comes to divide each MREI-like TO branch into four quasiparallel TO subbranches. The intensity of a given TO Raman line due to a given bond, e.g., A-C, scales as the related bond fraction, i.e., as $1 - x$, weighted by the fraction of the corresponding first-neighbor three-dimensional host cluster as derived from a simple binomial law [5].

Altogether, the MREI (1-bond $\rightarrow$ 1-mode scheme) and cluster (1-bond $\rightarrow$ 4-mode scheme) models summarize the state-of-the-art backscattering-Raman and infrared spectra of zincblende alloys at the beginning of the previous decade, whereas a novel class of zincblende alloys has emerged, involving light second-row elements from the periodic table in isovalent substitution, such as Be, B, and N. These light elements form shorter bonds, often of less ionic character than those they substitute [28]. We emphasize that ionicity affects the noncentral (bending type) bond force constants [29], and thus the stability of the lattice under inherent bond distortion needed to accommodate locally the contrast in bond length of the coexisting species. For example, in (Zn,Be)Se the contrasts in length and ionicity of the Zn-Se and Be-Se bonds are as large as $\sim 9\%$ and $\sim 43\%$ [12], whereas in (Zn,Be)Te the corresponding contrasts reach $\sim 10\%$ and $\sim 60\%$ [12], respectively [11]. Such large contrasts generate locally dramatic bond distortions, giving rise to exacerbated phonon properties. (Zn,Be)-chalcogenides are particularly interesting among such highly contrasted alloys because they constitute the only known exception to demixing on moving away from the dilute limits. Their high-quality, i.e., not segregating, crystals can be grown throughout the entire composition domain [30,31], whereas, e.g., the N incorporation in GaAs [32] or B

incorporation in GaN [33] are currently limited to a few percent. As such, (Zn,Be)-chalcogenides offer a unique opportunity to refine the understanding of the vibration properties of zincblende alloys beyond both the MREI and cluster schemes.

In fact, a careful backscattering-Raman study of the (Zn,Be)Se alloy over the past decade [3] has revealed a disconcerting phonon pattern, corresponding to three [1$\times$ (Zn-Se),2$\times$ (Be-Se)] well-resolved TO modes for the alloy, as already mentioned (Sec. I). The long Zn-based bond gives a unique TO$_{\text{Zn-Se}}$ mode, as expected within the traditional MREI description. This indicates a basic insensitivity of the Zn-Se vibration to its local environment. In contrast, two distinct TO modes are resolved for the short Be-Se bond. When the alloy composition changes, the two Be-Se TO modes undergo quasiparallel shifts in between the limit frequencies of the parent BeSe mode ($x = 1$) and of the Be-impurity mode ($x \sim 0$). Regarding intensities, the basic MREI trend between the Zn-Se and Be-Se signals is globally preserved. However, within the Be-Se TO doublet, the dominant feature at one end of the composition domain turns minor at the other end, whereas the two features exhibit similar intensities at intermediate alloy composition ($x \sim 0.5$). The (Zn,Be)Te Raman pattern has similar characteristics [34].

Such a BeSe-like bimodal pattern (1-bond $\rightarrow$ 2-mode scheme) observed in the backscattering TO Raman spectra of (Zn,Be)Se clearly falls beyond the scope of the MREI model (1-bond $\rightarrow$ 1-mode), whereas the cluster model (1-bond $\rightarrow$ 4-mode scheme) seems overparametrized. It was exactly in this context that the aforementioned percolation model was initially proposed [3]. Its starting point is a distinction between two possible (Zn-like or Be-like) first-neighbor environments of the Be-Se bond. In a recent development, care was taken to define such environments at one dimension [6], which is consistent with the spirit of the linear chain approximation upon which the percolation scheme relies (differently from a three-dimensional formulation seen with the cluster model). The resulting one-dimensional Be-Se oscillators are Se (Be-Se) Be and Se (Be-Se) Zn, corresponding to the TO$_{\text{Be-Se}}^{\text{Be}}$ and TO$_{\text{Be-Se}}^{\text{Zn}}$ modes. In the latter compact notation, the subscript refers to a given bond vibration in a given one-dimensional environment whose composition (Be- or Zn-like) is specified via the (Be,Zn) superscript [6]. In a frequency vs composition plot, the percolation scheme splits the unique TO$_{\text{Be-Se}}$ branch of the MREI scheme into two quasiparallel (TO$_{\text{Be-Se}}^{\text{Be}}$, TO$_{\text{Be-Se}}^{\text{Zn}}$) subbranches, ranked in order of increasing frequency. The percolation splitting parameter, i.e., the frequency gap between the two Be-Se TO branches, characteristic of the Be-Se bond in the Zn$_{1-x}$Be$_x$Se alloy appears to be as large as ~ 50 cm^{-1} (see below), corresponding to more than 10% of the frequency. This splitting parameter, important for the following, is denoted $\Delta_{\text{Be-Se}}$ hereafter. As for the Raman intensities of the (TO$_{\text{Zn-Se}}$, TO$_{\text{Be-Se}}^{\text{Be}}$, TO$_{\text{Be-Se}}^{\text{Zn}}$) modes, they are governed by the fractions of the related one-dimensional oscillators. For example, the intensity of the unique MREI-like Zn-Se mode simply scales as the Zn-Se bond fraction, i.e., as $1 - x$. The intensities of the two Be-Se modes scale as the probabilities of finding Be next to Be in a linear description of the crystal in reference to the Se (Be-Se) Be one-dimensional oscillator (TO$_{\text{Be-Se}}^{\text{Be}}$) and of finding Be next to Zn in reference to the Se (Be-Se) Zn

one-dimensional oscillator (TO_{Be-Se}^{Zn}), i.e., as $f_{Be-Se}^{Be} = x^2$ and $f_{Be-Se}^{Zn} = x \cdot (1 - x)$, respectively. All the above probabilities are estimated assuming a random Zn $\leftrightarrow$ Be substitution.

IV. COMBINED EXPERIMENTAL/THEORETICAL STUDY OF THE LATTICE DYNAMICS OF THE $\mathbf{Zn_{1-x}Be_xSe}$ ALLOY OVER THE ENTIRE BZ

In this section, we report an experimental and theoretical study of the three-mode [1× (Zn-Se),2× (Be-Se)] behavior of the $Zn_{0.67}Be_{0.33}Se$ alloy in its $\vec{q}$-dependence throughout the entire BZ, with special attention to the BeSe-like TO doublet. In Sec. IIIA, a reference insight near Γ is first achieved by combining Raman scattering and *ab initio* calculations. In Sec. IIIB, we explore the vibration properties of the $Zn_{0.67}Be_{0.33}Se$ alloy away from Γ up to the zone edge by INS, along the [001], [110], and [111] high-symmetry directions of the BZ. Comparison is done with SIESTA calculations of the $\vec{q}$-resolved Ph-DOS and with the shell-model results.

A. Reference Raman/*ab initio* insight into the Be-Se doublet near Γ

1. The Be-Se (TO,LO) Raman picture

We show in Fig. 2(a) the pure TO Raman spectrum recorded in geometry 1 by using the 633.0-nm laser line with the (110)-oriented $Zn_{0.67}Be_{0.33}Se$ single crystal studied by INS. The ($TO_{Be-Se}^{Be,1}$, $TO_{Be-Se}^{Zn,1}$) doublet shows up distinctly, characterized by both a large splitting Δ_{Be-Se} (~50 cm^{-1}) and comparable intensities of the two BeSe-like Raman features. In contrast, a unique MREI-like TO_{Zn-Se} mode is detected ($\Delta_{Zn-Se} \sim 0$ cm^{-1}). A complementary pure-LO Raman insight at a similar composition, shown in Fig. 2(b) (upper experimental curve), is obtained by analyzing the ~1-μm-thick $Zn_{0.69}Be_{0.31}Se$ epilayer in geometry 2. The corresponding pure-TO Raman spectrum, taken in geometry 1′, is also shown (lower experimental curve), shifted beneath the LO spectrum. This ensures a consistent discussion on a common TO basis of the two separate series of Raman spectra recorded with the large size ingot [Fig. 2(b)] on the one hand and with the epilayer [Fig. 2(b)] on the other hand. In fact, the two TO Raman spectra look similar regarding not only the frequencies of the ($TO_{Be-Se}^{Be,1}$, $TO_{Be-Se}^{Zn,1}$) modes but also their linewidths and relative intensities. A quantitative comparison is developed hereafter.

A decisive insight into the nature of the Zn $\leftrightarrow$ Be substitution in each sample, an especially important one for the $Zn_{0.67}Be_{0.33}Se$ single crystal studied by INS, can be achieved from careful line profile modeling of the corresponding pure-TO three-mode (TO_{Zn-Se},TO_{Be-Se}^{Be},TO_{Be-Se}^{Zn}) Raman lineshapes using Eq. (1), with special attention paid to the intensity ratio between the two Be-Se modes. We have discussed in detail elsewhere [15] that this ratio is extremely sensitive to local clustering or anticlustering.

Satisfactory line profile modeling of the three-mode (TO_{Zn-Se},TO_{Be-Se}^{Be},TO_{Be-Se}^{Zn}) Raman spectrum earlier recorded by using the 514.5-nm laser excitation in geometry 1 with the $Zn_{0.67}Be_{0.33}Se$ single crystal was carried out in Ref. [16] under the assumption of a random Zn $\leftrightarrow$ Be substitution. Under these circumstances, the intensity ratio between the
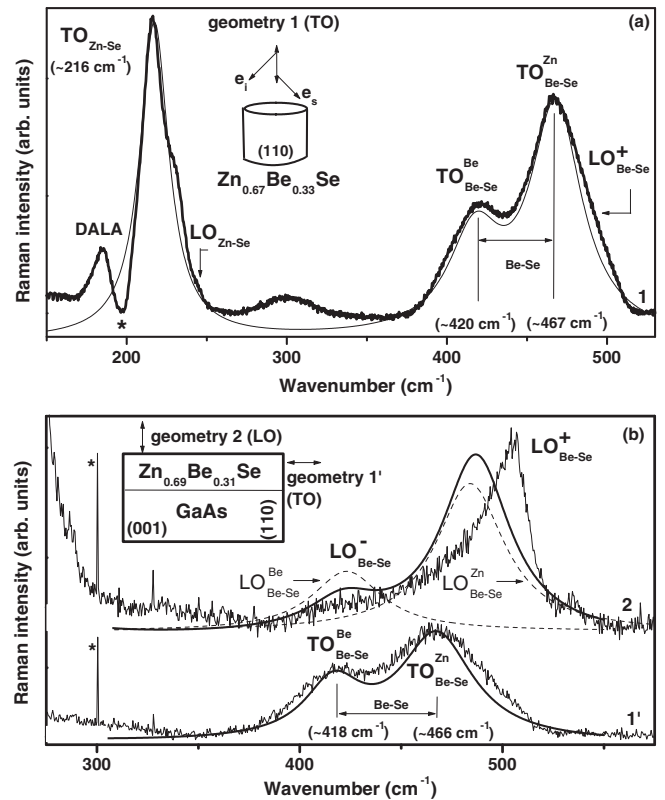
FIG. 2. Room-temperature Raman spectra taken (a) with the $Zn_{0.67}Be_{0.33}Se$ single crystal studied by INS by using the 633.0-nm He-Ne laser line in the pure-TO geometry corresponding to backscattering along the [110]-growth axis (refer to the double arrow) with crossed incident ($\vec{e_i}$) and scattered ($\vec{e_s}$) polarizations (geometry 1) and (b) with the $Zn_{0.69}Be_{0.31}Se$ epitaxial layer by using the 514.5-nm Ar+ laser line in pure-LO and pure-TO geometries, corresponding to backscattering along the [001]-growth (geometry 2) and [110]-edge (geometry 1′) crystal axis (refer to the double arrow), respectively. Corresponding theoretical percolation-type TO- and LO-coupled (solid lines) and LO-uncoupled (dashed lines) Raman spectra calculated based on a random Zn $\leftrightarrow$ Be substitution are superimposed for comparison. The stars mark a Fano interference between the theoretically forbidden DALA band and the TO_{Zn-Se} mode (a) and a parasitical laser line (b).

experimental TO_{Be-Se}^{Be} and TO_{Be-Se}^{Zn} modes appeared to scale at the ratio of 1:2. This is the ratio predicted when considering the nominal fractions of 1D oscillators behind such TO modes, as established in Sec. III (refer to the f terms) on the basis of a random Zn $\leftrightarrow$ Be substitution. The remaining adjustable parameters are the phonon frequencies and corresponding damping (specified within parentheses hereafter), chosen as follows: 216.2 (10); 423.5 (40); and 468.5 (40) cm^{-1}.

The same theoretical TO Raman spectrum as that calculated in Ref. [16] is presently superimposed in Fig. 2(a) onto the pure-TO experimental $Zn_{0.67}Be_{0.33}Se$ Raman spectrum, also taken in geometry 1 by using the alternative 633.0-nm laser line. The latter spectrum is of better quality than that reported in Ref. [16] since the parasitic LO contribution is totally absent. Again, the agreement between experiment and theory is good, which confirms that the Zn $\leftrightarrow$ Be substitution is random in the large-sized $Zn_{0.67}Be_{0.33}Se$ crystal studied by INS.

Imperfections in the TO line profile modeling are either due to reminiscent LO signals [theoretically forbidden, hardly observable, and indicated by broken arrows in Fig. 2(a)] or to a Fano interference involving disorder-activated longitudinal acoustic (DALA) modes, as observed by characteristic antiresonance in Fig. 2(a) (refer to the star) [3]. A similar agreement between the experimental (thick lines) and theoretical (thin curves) TO Raman lineshapes of the $Zn_{0.69}Be_{0.31}Se$ epilayer is also achieved under the assumption of a random $Zn \leftrightarrow Be$ substitution, as observed by the nominal 1:2 intensity ratio between the two observed BeSe-like TO modes, using the following sets of phonon frequencies (corresponding dampings in parentheses): 216.5 (14); 417.0 (44); 468.0 (34) cm^{-1}. The two curves are superimposed at the bottom of Fig. 2 for a direct comparison.

Using the above TO analysis, we may conclude that both the $Zn_{0.67}Be_{0.33}Se$ single crystal and the $Zn_{0.69}Be_{0.31}Se$ epilayer are random alloys.

Now we turn to the LO modes, shown at the top of Fig. 2(b), for the sake of completeness. Based on the analogy between the TO Raman spectra of our two samples, we may safely infer, in crude approximation, that the pure-LO Raman spectrum recorded with the $Zn_{0.69}Be_{0.31}Se$ epilayer is also representative of the $Zn_{0.67}Be_{0.33}Se$ single crystal studied by INS.

The striking feature in the LO symmetry is the dramatic effect of the macroscopic $\vec{E}$ coupling. In fact, the macroscopic fields of the $LO_{Be-Se}^{Be,1}$ and $LO_{Be-Se}^{Zn,1}$ modes directly associated with the corresponding $TO_{Be-Se}^{Be,1}$ and $TO_{Be-Se}^{Zn,1}$ counterparts couple so strongly that most of the available BeSe-like oscillator strength is channeled toward a unique, giant LO_{Be-Se}^{+} oscillation at high frequency, leaving behind a residual overdamped LO_{Be-Se}^{-} mode repelled close to the $TO_{Be-Se}^{Be,1}$ mode. Such spectacular $\vec{E}$-mediated transfer of oscillator strength was extensively studied in Ref. [3]. We emphasize that, due to the $\vec{E}$ coupling, neither $LO_{Be-Se}^{Be,1}$ nor $LO_{Be-Se}^{Zn,1}$ can be observed experimentally; only the (minor, dominant) $\vec{E}$-coupled $(LO_{Be-Se}^{-}, LO_{Be-Se}^{+})$ doublet is accessible. This justifies our motivation to focus most of our attention in this paper on the purely mechanical TO modes.

The theoretical LO Raman lineshape of the $Zn_{0.69}Be_{0.31}Se$ epilayer, with a characteristic $(LO_{Be-Se}^{-}, LO_{Be-Se}^{+})$ doublet of $\vec{E}$-coupled modes, obtained via Eq. (1) by using the same set of input parameters as used for the line profile modeling of the corresponding pure-TO Raman spectrum (refer to discussion above), is superimposed to the experimental signal at the top of Fig. 2(b). The underlying uncoupled $LO_{Be-Se}^{Be,1}$ and $LO_{Be-Se}^{Zn,1}$ theoretical Raman modes (dashed curves) taken independently, thus coming as two separate lines, are also shown for a better appreciation of the distortion of the original LO signal due to $\vec{E}$ coupling and for help in the discussion of the INS data at a later stage. The Raman lineshapes of such uncoupled LO_{Be-Se}^{Be} and LO_{Be-Se}^{Zn} modes were calculated by reducing artificially the expression of $\varepsilon_r(\omega, x)$ to the corresponding individual oscillator in the calculation of the LO RCS. Note that the experimental LO_{Be-Se}^{+} line is shifted to a significantly higher frequency than the theoretical prediction. This is due to a discrete fine structure of the uncoupled LO_{Be-Se}^{Be} and LO_{Be-Se}^{Zn} modes induced by the alloy disorder, as extensively discussed in Ref. [3]. In contrast, the TO modes

remain unaffected by such multimode fine structuring, also discussed in Ref. [3].

Summarizing, the TO Raman spectra of the single crystal plus the LO one from the epilayer together provide a reasonable insight into the optic mode behavior of the random $Zn_{0.67}Be_{0.33}Se$ single crystal near Γ at room temperature. This provides a firm basis for analyzing the (TO, LO) dispersion in this sample by INS at low temperature in Sec. IVB.

2. *Ab initio insight near* Γ *into the microscopic origin of* Δ_{Be-Se}

The microscopic origin of the percolation splitting Δ_{Be-Se} observed between the $TO_{Be-Se}^{Be,1}$ and $TO_{Be-Se}^{Zn,1}$ Raman modes is probed in *ab initio* calculations of the Γ-projected Ph-DOS per Be atom performed with a $Be_2Zn_{30}Se_{32}$ supercell, simulating the simplest percolation-type Be-impurity motif at hand, namely a pair of connected Be-Se bonds [6], noted –Be–Se– Be– hereafter, inserted in bulk ZnSe. We can imagine two possible reasons behind the splitting: the lifting of degeneracy of impurity-related modes due to a mere symmetry lowering (another impurity being nearby), and the effect of local lattice relaxation [35], as needed to accommodate the contrast in the Zn-Se and Be-Se bond lengths around that motif.

To probe the two mechanisms separately, *ab initio* phonon calculations on the supercell in question were done with and without the bond-length relaxation in the Be-pair frag-ment [36]. The resulting Γ-projected Ph-DOS per Be atom is shown in Fig. 3. Interestingly, the vibration modes of
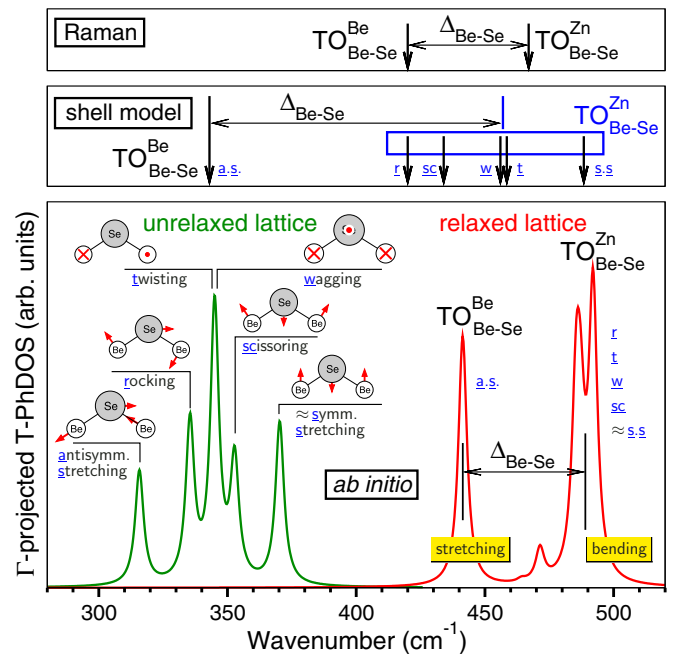
FIG. 3. (Color online) *Ab initio* Γ-projected T–Ph-DOS per Be atom of the –Be–Se–Be– motif inserted in a ZnSe-like (64-atom) supercell, as obtained at 0 K with (red line, on the right) and without (green line, on the left) relaxation. The individual vibration patterns, schematically shown, are labeled in standard notation (as for the –CH_2– methylene group). Corresponding vibration frequencies obtained for the same –Be–Se–Be– motif within the shell model are indicated in the middle panel. The experimental BeSe-like TO Raman frequencies (taken from Fig. 2) are shown in the top panel.

the –Be–Se–Be– motif resemble the Raman active modes of similar –CH$_2$– methylene groups connected via their C-backbone into quasilinear pseudoinfinite paraffin chains. We thus adopt the established chemical notation of rocking ($r.$), twisting ($t.$), wagging ($w.$), scissoring ($sc.$), symmetrical stretching ($s.s.$), and antisymmetrical stretching ($a.s.$) [37]. The individual vibration patterns are schematically shown in Fig. 3. Still, the methylene and Be series differ with respect to the stretching modes. Indeed the symmetrical stretching acquires a pronounced bending character in the Be series (refer to the schematic vibration pattern in Fig. 3), whereas the antisymmetrical stretching, the hardest mode of the methylene series, identifies with the softest mode of the Be series.

When neglecting the lattice relaxation (which can be carried out only in a specially configured computer experiment but not in the real case), the Be-induced local tensile strain, not accommodated locally, leads to a spectacular phonon softening. More interestingly, without relaxation the different phonon symmetries induce a series of evenly spaced modes. If a realistic phonon damping of 10–20 cm^{-1} is taken into account, the whole series may give an impression of a unique MREI-like feature ($\Delta_{\text{Be-Se}} \sim 0$ cm^{-1}). In contrast, with relaxation, the modes condense into two clearly separated entities ($\Delta_{\text{Be-Se}} \sim 50$ cm^{-1}): the pure stretching mode ($a.s.$), on the one hand, and the remaining modes of the series ($r.$, $t.$, $w.$, $sc.$, $s.s.$), all with at least partial bending character, on the other hand. This provides an unambiguous theoretical insight into the origin of the percolation splitting $\Delta_{\text{Be-Se}}$, as observed in the Raman spectra (top inset in Fig. 3) [38].

Note that the ($r.$, $t.$, $w.$, $sc.$, $s.s.$, $a.s.$) Be-impurity modes cannot be described in terms of nominal $q \sim 0$ Raman-allowed modes, in which all cations are expected to vibrate in phase as a quasirigid sublattice (recall the quasi-infinite wavelength). They rather assimilate with zone-edge modes. Indeed, the in-phase vibration of cations is strictly limited to the Be-impurity motif itself, i.e., at the scale of merely two interatomic distances, becoming overdamped as soon as penetrating the surrounding ZnSe-like host medium. The reason is simply that the Zn-Se bonds do not naturally vibrate at the same frequency as the Be-Se ones (as apparent, e.g., in Fig. 2), thus constituting a natural obstacle to the propagation of the foreign Be-like mode. Based on such consideration, we expect that the frequency gap $\Delta_{\text{Be-Se}}$ between the TO$_{\text{Be-Se}}^{\text{Be,1}}$ and TO$_{\text{Be-Se}}^{\text{Zn,1}}$ modes should remain visible up to the BZ edge. This was confirmed by INS measurements (see the next section).

We use the well-characterized vibration pattern of the prototype percolation-type Be-pair fragment in ZnSe, as determined by *ab initio* simulations above, to test the transferability of the shell model to the (Zn,Be)Se alloy. As expected, the diagonalization at $\vec{q} = \vec{0}$ of the dynamical matrix of the cubic $2 \times 2 \times 2$ Zn$_{30}$Be$_2$Se$_{32}$ supercell obtained using the shell model provides six distinct vibration modes for the Be pair. The corresponding vibration frequencies are indicated by arrows in the intermediary inset of Fig. 3. As expected, the individual vibration pattern behind each frequency matches the *ab initio* references. The vibration patterns are thus classified using the same terminology of $a.s.$, $r.$, $t.$, $w.$, $sc.$, and $s.s$. The important point is that on one hand, the shell model provides the expected distinction between the $a.s.$ at low frequency, and, on the other

hand, all possible variants in bending of the –Be–Se–Be– chain regrouped at a higher frequency. This was a *sine qua non* condition to validate the shell model for the discussion of the forecoming Zn$_{0.67}$Be$_{0.33}$Se INS data in the next section.

We must admit, though, that some differences exist between the percolation doublets generated *ab initio* and via the shell model for the –Be–Se–Be– impurity motif. These relate to the phonon frequencies. For example, while the bendinglike ($r.$, $t.$, $w.$, $sc.$, $s.s.$) multiplet remains quasidegenerated in the *ab initio* vibration pattern, it divides into a discrete series of vibration modes in the corresponding pattern obtained via the shell model. Moreover, the shell model overestimates the Raman/*ab initio* percolation splitting $\Delta_{\text{Be-Se}}$ roughly by a factor of two. This may be due to the lack of angular dependence of the used potential, which thus fails to account for change in the bond force constant due to inherent bond distortion "in shear" in an alloy, or to intrinsic limitations of the shell model being already responsible for the apparent doubling of the magnitude of the TO-LO splitting in the theoretical phonon dispersion curves related to the parent ZnSe and BeSe compounds (see Sec. II). Nevertheless, reliable qualitative trends can be inferred from the shell model, which is sufficient for our use.

B. Lattice dynamics of Zn$_{0.67}$Be$_{0.33}$ outside Γ—INS and lattice dynamics calculations (*ab initio*, shell model)

The above discussion concerning the Be-impurity pair implies that the two-mode percolation-type splitting $\Delta_{\text{Be-Se}}$, an essential feature of the percolation model, ought to survive somehow away from Γ. In the following, we directly address the issue of how exactly this presumably two-mode behavior throughout the BZ manifests itself.

1. Preliminary ab initio insight along Γ → X

Preliminary insight into the $\vec{q}$-dependence of $\Delta_{\text{Be-Se}}$ can be obtained by *ab initio* calculations. We use the two large (192-atom) $6 \times 2 \times 2$ Zn$_{0.67}$Be$_{0.33}$Se disordered supercells, tripled along the [100] crystal axis, labeled as supercells 1 and 2 in Sec. IIC to obtain the calculations. The corresponding q_x-dependent T–Ph-DOS (dark curves) and L–Ph-DOS (clear curves) per Zn (left side) and Be (right side) atom, each mode being modeled by a damped Lorentzian function with linewidth at half height of 4 cm^{-1}, are shown in Fig. 4, in top and bottom positions, respectively. The BZ edge (X) roughly corresponds to $q_x = 0.18$ Bohr^{-1}. This is confirmed by a reversal of the phonon dispersion curves marking the entry into the second BZ. Generally, the overall trends in the two panels of Fig. 4 are similar, notably in what concerns the bimodal pattern of the BeSe-like TO response, with some differences in details.

A single acoustic mixed mode, implying both Zn-Se and Be-Se vibrations, is observed, as in earlier theoretical works [8,9]. Careful examination reveals that Be is much less involved than Zn in the transverse acoustic mode, while the longitudinal acoustic mode appears to be dominated by the Se vibration.

A clear decoupling between the Zn-Se and Be-Se vibrations occurs in the optic range, the long and ionic Zn-Se bond
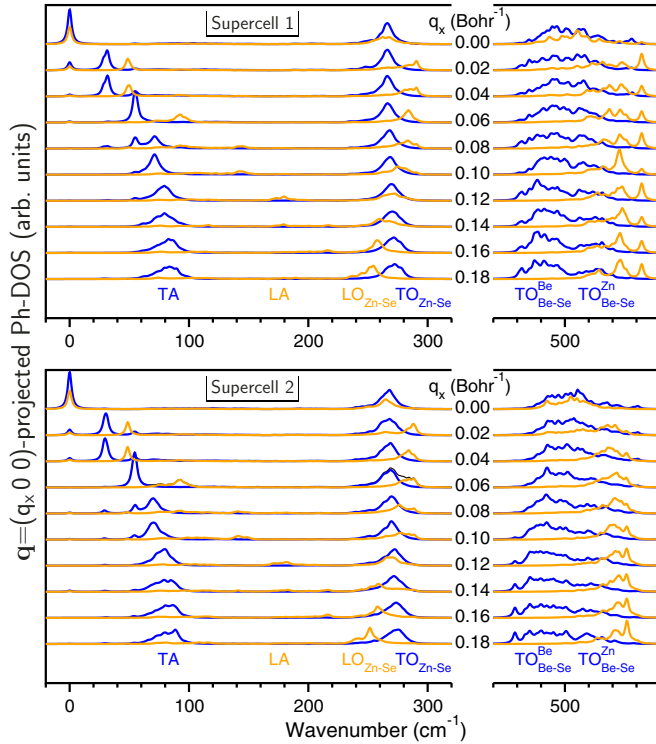
FIG. 4. (Color online) Transversal (dark blue lines) and longitudinal (yellow lines) components in the density of modes calculated using the *ab initio* SIESTA code over two different special quasirandom 192-atom supercells (upper and lower panels), describing the $Zn_{0.67}Be_{0.33}Se$ solid solution. Densities of modes are further resolved in the values of the wavevector, chosen to scan the dispersion from Γ to X.

vibrating at much lower frequency (~ 250 cm^{-1}) than the shorter and more covalent Be-Se one (~ 500 cm^{-1}). An overall blue shift of the Γ-projected (TO,LO) Ph-DOS with respect to the corresponding Zn-Se and Be-Se Raman signals of ~ 25 cm^{-1}, as apparent in Fig. 3, is due to a well-known bias of the local density approximation leading to artificial strengthening of the chemical bonds. Another source of discrepancy near Γ may be that the *ab initio* calculations are done at 0 K, while the experimental Raman spectra were taken at 300 K.

Away from Γ, the *ab initio* calculations predict a unique and narrow (TO_{Zn-Se}, LO_{Zn-Se}) MREI-like mode throughout the BZ, as actually observed near Γ in the experimental Raman spectra (see Fig. 2). Note that the *ab initio* TO_{Zn-Se} mode remains nearly dispersionless along $\Gamma \rightarrow X$, while the *ab initio* LO_{Zn-Se} mode exhibits a marked negative dispersion. This leads to LO-TO inversion approximately halfway along $\Gamma \rightarrow X$. Now we turn to the Be-Se signal, which occupies most of our attention in this paper. A single LO band is detected for Be-Se throughout the whole BZ, with some fine structuring on its low-frequency side. Altogether, this strongly reminds us of the asymmetric dominant LO_{Be-Se}^+ Raman signal [see Fig. 2(b)]. Expectedly, the Be-Se TO signal is not as simple. A broad band with considerable fine structure, hardly comparing with the Raman doublet in the vicinity of Γ, gradually takes shape for increasing q_x values along [100], eventually stabilizing close to X into a distinct and nearly dispersionless bimodal

pattern familiar from Raman spectra. Basically, the Be-Se TO percolation doublet seems to survive at finite wavelength, with even better resolution than at Γ. This is encouraging in view of a possible detection by INS. Note that neither the BeSe-like TO mode nor its LO counterpart seem to exhibit any dispersion along $\Gamma \rightarrow X$.

2. *Ph-DOS and phonon dispersion of the* $Zn_{0.67}Be_{0.33}Se$ *alloy—INS and shell model*

An overview into the phonon behavior of the $Zn_{0.67}Be_{0.33}Se$ alloy, integrated over the whole BZ, is obtained by measuring its Ph-DOS at 13 K by INS using the powder sample. Experimental details are given in Sec. IIB. The resulting INS spectrum is shown in Fig. 5 (circles). In spite of the fact that Be is less abundant than Zn in $Zn_{0.67}Be_{0.33}Se$, the INS signal shows up more strongly for Be-Se than for Zn-Se, in contrast with Raman findings [see Fig. 2(a)]. This is due to the enhanced neutron scattering efficiency of the light Be element as compared to Zn. The corresponding theoretical Ph-DOS at 13 K, computed within the shell model along the procedure detailed in Sec. IIC, is superimposed to the INS experimental curve (thin line) for comparison. The agreement between experiment and theory is globally good, at least in the spectral range of the optical modes, apart from one significant discrepancy concerned with the minor feature produced at ~ 340 cm^{-1} by the shell model [Fig. 5; refer to the star]. This has no counterpart in the experimental INS spectrum. Such a parasitical signal is due to the theoretical $TO_{Be-Se}^{Be,1}$ mode, which is over redshifted in the shell model with respect to the experiment, as already discussed in Sec. IVA2. Nevertheless, in a first approximation, the shell model can be used to assign the main features of the experimental Ph-DOS.

Three main features are identified in the Ph-DOS, i.e., a narrow peak at ~ 100 cm^{-1}; a broader one at ~ 220 cm^{-1}, with a full width at half maximum of ~ 40 cm^{-1}; and a much broader one characterized by a bimodal pattern, centered at ~ 460 cm^{-1}, spreading over ~ 125 cm^{-1}. Based on the Raman data, on the shell model and also on a qualitative comparison
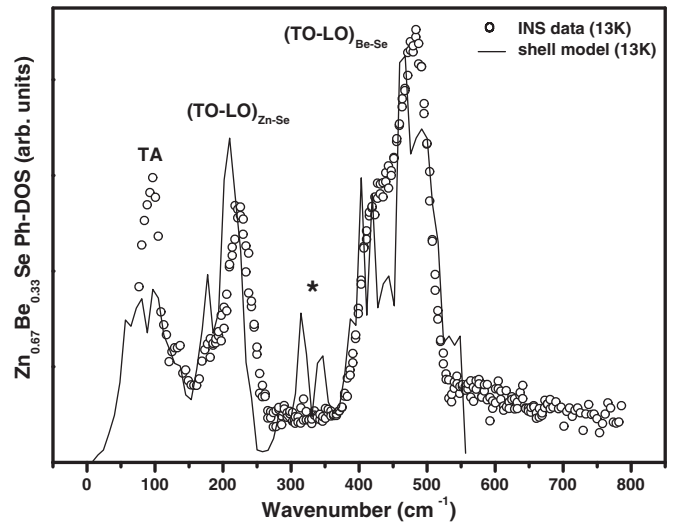
FIG. 5. Ph-DOS measured by INS at 13 K with the $Zn_{0.67}Be_{0.33}Se$ powder (circles). The theoretical Ph-DOS calculated via the shell model at 13 K is superimposed (solid curve) for comparison.

with the *ab initio* $\vec{q}$-projected (T,L)–Ph-DOS displayed in Fig. 4, such features are assigned as follows. The narrow peak at ~ 100 cm^{-1} comes from the transverse acoustic modes, which tend to become nearly dispersionless near the BZ edge (see Fig. 4), with a large Ph-DOS. Such phenomenon, already seen in the phonon dispersion curves of the parent ZnSe and BeSe compounds (see Fig. 1), was earlier observed for Ga$_{0.5}$Al$_{0.5}$As by Baroni *et al.* [9]. The broader feature at ~ 220 cm^{-1} is due to the rather narrow ZnSe-like TO-LO band, covering less than ~ 40 cm^{-1}. A clear insight near Γ is given in Fig. 2(a). Last, the extended Ph-DOS with a bimodal pattern centered at ~ 460 cm^{-1} originates from the BeSe-like TO-LO band, much broader than the ZnSe-like counterpart, as clearly apparent in Figs. 2(b) and 4. In fact, when referring back to the Raman insight near Γ displayed in Fig. 2(b), we may infer that the low- and high-frequency features constituting the experimental BeSe-like bimodal Ph-DOS may result on one hand from the added contributions of the neighboring TO$_{\text{Be-Se}}^{\text{Be}}$ and LO$_{\text{Be-Se}}^{-}$ modes and on the other hand from the added contributions of the neighboring TO$_{\text{Be-Se}}^{\text{Zn}}$ and LO$_{\text{Be-Se}}^{+}$ modes. However, when confronted directly with such experimental Ph-DOS, one may as well presume *a priori* that the bimodal BeSe-like Ph-DOS merely reflects separate contributions from the BeSe-like TO and LO modes in a crude MREI-like (1-bond $\rightarrow$ 1-mode) description of the BeSe-like lattice dynamics of the Zn$_{0.67}$Be$_{0.33}$Se alloy. The measured BeSe-like Ph-DOS is thus not decisive regarding the existence, or not, of the finite frequency gap $\Delta_{\text{Be-Se}}$ between the TO$_{\text{Be-Se}}^{\text{Be}}$ and TO$_{\text{Be-Se}}^{\text{Zn}}$ modes outside Γ. A specific TO insight is needed to decide.

Separate INS insights into the BeSe-like TO and LO dispersions were achieved by using the Zn$_{0.67}$Be$_{0.33}$Se single crystal. Different $\vec{q}$ points along the [100], [011], and [111] high-symmetry directions were probed at 13 K. The $\vec{q}$ points in question were selected after computer simulation of the $\vec{q}$-dependent INS cross section within the shell model, as explained in Sec. IIC. A selection of TO and LO INS spectra taken at well-spanned $\vec{q}$ points along the $\Gamma \rightarrow X$ [100] direction of the BZ is shown in Fig. 6.

Consistent with the *ab initio* calculations reported in Fig. 4, a single and narrow MREI-like TO$_{\text{Zn-Se}}$ mode shows up (see $q_x = 0.3$) in the INS spectra. In contrast, a distinct Be-Se percolation-type doublet is detected in both the TO and LO symmetries by INS throughout the whole BZ. Note that an assignment of the experimental BeSe-like features according to their TO-like or LO-like nature does not pose any problem, since they are clearly decoupled by symmetry (compare the top and bottom panels corresponding to $q_x = 0.5$ and $q_x = 0.8$ in Fig. 6).

The full set of INS frequencies measured at 13 K for the acoustic (squares) and optic (circles) modes in both the transverse (black symbols) and longitudinal (yellow-clear symbols) symmetries along the [100], [011], and [111] directions in reciprocal space (plain symbols) plus the corresponding TO Raman frequencies measured at 300 K (refer to Γ), added for sake of completeness, are displayed in Fig. 7. The theoretical dispersion curves obtained via the shell model are superimposed to the experimental INS data for comparison using an explicit grayscale. These were obtained by calculating the neutron scattering cross section at regularly spaced $\vec{q}$ points along the considered directions of the BZ and by introducing
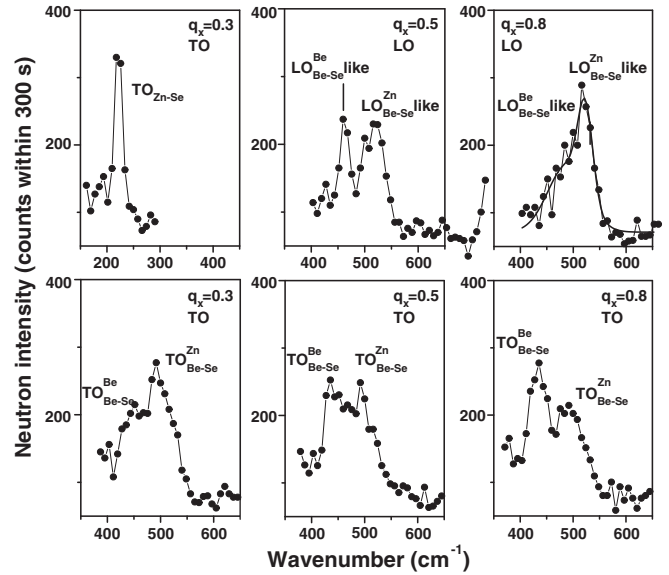
FIG. 6. Selection of TO and LO INS spectra taken at 13 K at well-spanned q_x values along $\Gamma \rightarrow X$ [100] in the Zn-Se (top left panel) and Be-Se (other panels) spectral ranges. At $q_x = 0.8$, the LO doublet is only resolved via a contour modeling of the INS profile (thick curve) using two Gaussian functions.

some artificial broadening along the energy axis to be able to plot each $\vec{q}$-cut as a continuous function of energy. The main experimental trends are well reproduced by the shell model regarding both the TO and LO modes, at least qualitatively.

It can be seen from Fig. 6 that the Be-Se TO splitting $\Delta_{\text{Be-Se}}$ survives almost unchanged throughout the whole BZ down to the shortest wavelengths (near X, K, and L) in all examined directions of the BZ. This provides decisive experimental support to our view that such TO doublet finds its origin at the ultimate bond scale, as anticipated from the lattice dynamics calculations performed with the short percolation-type –Be–Se–Be– prototype Be-impurity motif (see Sec. IVA2). Altogether, such consistent theoretical and experimental insights secure a basic assumption behind the percolation scheme that the splitting $\Delta_{\text{Be-Se}}$ distinguishes between different environments of a bond (either of the Be type or of the Zn type; see Sec. III) at the very local scale.

The LO decoupling occurs away from Γ on account of the emergence of the LO$_{\text{Be-Se}}^{\text{Be}}$ mode as a distinct INS feature along $\Gamma \rightarrow X$, as clearly apparent at $q_x = 0.5$ (see Fig. 6). For comparison, a limiting case of full LO decoupling near Γ is shown in Fig. 2(b), in reference to the theoretical uncoupled LO$_{\text{Be-Se}}^{\text{Be}}$ and LO$_{\text{Be-Se}}^{\text{Zn}}$ Raman lines (dotted curves). Eventually the LO$_{\text{Be-Se}}^{\text{Be}}$ mode appears to converge onto the LO$_{\text{Be-Se}}^{\text{Zn}}$ one when approaching X. Indeed the LO doublet at $q_x = 0.8$ could be resolved only via a double-Gaussian line shape fit to the data (superimposed to the INS data in the top right panel of Fig. 6).

A yet unexplained disturbing feature is that the intensity ratio between the TO$_{\text{Be-Se}}^{\text{Be}}$ and TO$_{\text{Be-Se}}^{\text{Zn}}$ INS modes drastically changes while progressing along $\Gamma \rightarrow X$. While the TO$_{\text{Be-Se}}^{\text{Zn}}$ INS mode dominates its TO$_{\text{Be-Se}}^{\text{Be}}$ counterpart by a factor of nearly two near Γ (refer to $q_x = 0.3$ in Fig. 6), as
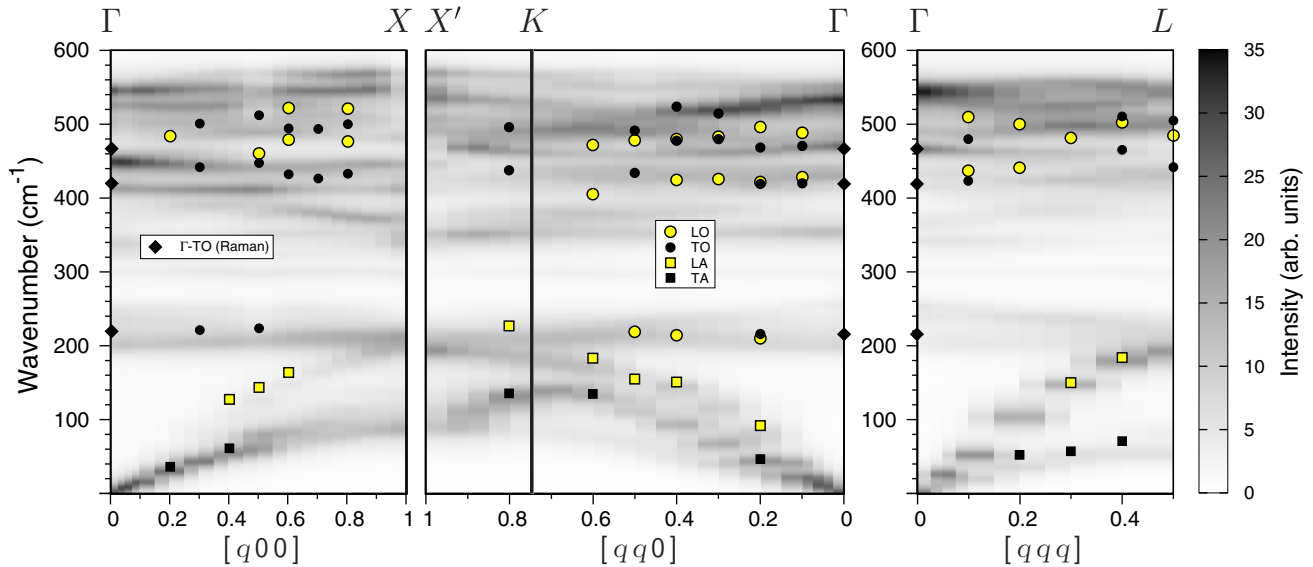
FIG. 7. (Color online) Acoustic (squares) and optic (circles) phonon frequencies of the $Zn_{0.67}Be_{0.33}Se$ single crystal measured by INS (circles and squares) at 13 K at different $\vec{q}$ wavevectors along the usual high-symmetry directions in reciprocal space in both the transverse (black symbols) and longitudinal (yellow-clear symbols) symmetries. The TO Raman frequencies (at Γ, black diamonds) observed at 300 K are added for the sake of completeness. The theoretical phonon dispersion curves, as inferred from direct calculation of the neutron scattering cross section of $Zn_{0.67}Be_{0.33}Se$ via the shell model, are also shown using an explicit grayscale (refer to the right) for comparison.

also observed in the Raman spectra (refer to Fig. 1), the intensity ratio is inverted near the zone edge (refer to $q_x = 0.8$ in Fig. 6). Interestingly, the dominance of TO_{Be-Se}^{Be} near the zone edge is also apparent in the Be-related *ab initio* T–Ph-DOS calculated with both supercells 1 and 2 (see Fig. 4). This cannot be merely fortuitous; however, even a careful examination of the vibration patterns behind the *ab initio* TO_{Be-Se}^{Be} and TO_{Be-Se}^{Zn} T–Ph-DOS was thus far not helpful in elucidating the reason for such inversion. If we refer to the absolute neutron intensities (see Fig. 6) and transpose the discussion within the percolation scheme, it seems that the "in-chain" Be-Se stretching (*a.s.*) of connected Be-Se bonds, in reference to TO_{Be-Se}^{Be}, becomes somehow enhanced at short wavelength, whereas the "out-of-chain" Be-Se bending (including *r.*, *t.*, *w.*, *sc.*, *s.s.*), in reference to TO_{Be-Se}^{Zn}, gets partially inhibited. In a linear description of the crystal at one dimension along the linear chain approximation, when the wavelength reduces, the Be-Se bonds tend to stretch more easily in their own environment, i.e., Be-like, than in the foreign Zn-like one. The reason for such behavior is not yet clear.

The primary motivation for the study, to prove whether the two BeSe-like TO modes forming the percolation doublet persist away from Γ, was satisfied in positive sense. Namely, the percolation doublet was predicted to exist up to the BZ edge in *ab initio* and shell-model calculations and was indeed experimentally detected up to this limit by INS. This reveals that the origin of splitting is at the ultimate bond scale, as was independently confirmed in a simulation for a minimal prototype –Be–Se–Be– impurity motif immersed in ZnSe. An essential role of local lattice relaxation, which accommodates the contrast in length and ionicity between the coexisting bond species in an alloy, is demonstrated in shaping the 1-bond → 2-mode percolation behavior. Eventually, such bimodal behavior appears to distinguish between the stretching and bending modes of connected, i.e., percolative, bonds of the like species.

The present study of the lattice dynamics of $Zn_{0.67}Be_{0.33}Se$ by INS away from Γ completes a recent study, by near-forward Raman scattering in the close vicinity of Γ, of its phonon-polariton modes in the same alloy [16]. Together they provide an overview of the TO vibrations of an alloy, in their full diversity throughout the entire BZ.

V. CONCLUSION

Summarizing, we performed a thorough study by INS of the lattice dynamics of the three-oscillator [$1 \times$ (Zn-Se), $2 \times$ (Be-Se)] $Zn_{0.67}Be_{0.33}Se$ random zincblende alloy throughout the whole BZ. The insight thus gained was supported by a Raman analysis near Γ and by lattice-dynamical calculations done using the *ab initio* SIESTA code and a shell model. Most of the attention was focused on the TO symmetry, which, in contrast to LO, preserves the natural richness of the phonon pattern in such a complex system as an alloy.

[1] S. Adachi, *Properties of Semiconductor Alloys: Group-IV, III-V and II-VI Semiconductors*, Wiley Series in Materials for Electronic & Optoelectronic Applications (John Wiley & Sons, Chichester, UK, 2009).

[2] D. W. Taylor, in *Optical Properties of Mixed Crystals*, edited by R. J. Elliott and I. P. Ipatova (North-Holland, Amsterdam, 1988), pp. 35–132.

[3] O. Pagès, M. Ajjoun, T. Tite, D. Bormann, E. Tournié, and K. C. Rustagi, Phys. Rev. B **70**, 155319 (2004).

[4] I. F. Chang and S. S. Mitra, Adv. Phys. **20**, 359 (1971).

[5] H. W. Verleur and A. S. Barker, Jr., Phys. Rev. **149**, 715 (1966).

[6] O. Pagès, J. Souhabi, V. J. B. Torres, A. V. Postnikov, and K. C. Rustagi, Phys. Rev. B **86**, 045201 (2012).

[7] T. M. Giebultowicz, J. J. Rhyne, J. K. Furdyna, and P. Klosowski, J. Appl. Phys. **67**, 5096 (1990).

[8] S. C. Varshney, J. F. Vetelino, S. S. Mitra, and I. F. Chang, Phys. Rev. B **12**, 5912 (1975).

[9] S. Baroni, S. de Gironcoli, and P. Giannozzi, Phys. Rev. Lett. **65**, 84 (1990).

[10] Acoustical phonons in $(A,B)C$ zincblende alloys correspond to in-phase vibrations of two fcc sublattices, the (A,B)-substituting one moving along with the C-only one.

[11] N. E. Christensen, S. Satpathy, and Z. Pawlowska, Phys. Rev. B **36**, 1032 (1987).

[12] The percentages are obtained by dividing the difference between the values of the two parent compounds by the largest value out of these two.

[13] F. Firszt, S. Łęgowski, H. Męczyńska, J. Szatkowski, W. Paszkowicz, and K. Godwod, J. Cryst. Growth **184/185**, 1335 (1998).

[14] F. Plazaola, J. Flyktman, K. Sarinen, L. Dobrzyński, F. Firszt, S. Łęgowski, H. Męczyńska, W. Paszkowicz, and H. Reniewicz, J. Appl. Phys. **91**, 1647 (2003).

[15] O. Pagès, A. V. Postnikov, A. Chafi, D. Bormann, P. Simon, F. Glas, F. Firszt, W. Paszkowicz, and E. Tournié, Eur. Phys. J. B **73**, 461 (2010).

[16] R. Hajj Hussein, O. Pagès, F. Firszt, W. Paszkowicz, and A. Maillard, Appl. Phys. Lett. **103**, 071912 (2013).

[17] D. T. Hon and W. L. Faust, Appl. Phys. **1**, 241 (1973).

[18] T. Basak, M. N. Rao, and S. L. Chaplot, Physica B **407**, 4478 (2012).

[19] B. H. Lee, J. Appl. Phys. **41**, 2988 (1970).

[20] B. Jobst, D. Hommel, U. Lunz, T. Gerhard, and G. Landwehr, Appl. Phys. Lett. **69**, 97 (1996).

[21] R. G. Greene, H. Luo, and A. L. Ruoff, J. Phys. Chem. Solids **56**, 521 (1995).

[22] T. Basak, M. N. Rao, M. K. Gupta, and S. L. Chaplot, J. Phys.: Condens. Matter **24**, 115401 (2012).

[23] O. Pagès, M. Ajjoun, J. P. Laurenti, D. Bormann, C. Chauvet, E. Tournié, and J. P. Faurie, Appl. Phys. Lett. **77**, 519 (2000).

[24] G. P. Srivastava, H. M. Tutuncu, and N. Gunhan, Phys. Rev. B **70**, 085206 (2004).

[25] J. M. Soler, E. Artacho, J. D. Gale, A. García, J. Junquera, P. Ordejón, and D. Sánchez-Portal, J. Phys.: Condens. Matter **14**, 2745 (2002).

[26] A. V. Postnikov, O. Pagès, and J. Hugel, Phys. Rev. B **71**, 115206 (2005).

[27] S.-H. Wei, L. G. Ferreira, J. E. Bernard, and A. Zunger, Phys. Rev. B **42**, 9622 (1990).

[28] C. Vèrié, J. Cryst. Growth **184/185**, 1061 (1998).

[29] R. M. Martin, Phys. Rev. B **1**, 4005 (1970).

[30] C. Chauvet, E. Tournié, and J.-P. Faurie, Phys. Rev. B **61**, 5332 (2000).

[31] O. Maksimov and M. C. Tamargo, Appl. Phys. Lett. **79**, 782 (2001).

[32] J. Neugebauer and C. G. Van de Walle, Phys. Rev. B **51**, 10568 (1995).

[33] A. Ougazzaden, S. Gautier, T. Moudakir, Z. Djebbour, Z. Lochner, S. Choi, H. J. Kim, J.-H. Ryou, R. D. Dupuis, and A. A. Sirenko, Appl. Phys. Lett. **93**, 083118 (2008).

[34] O. Pagès, T. Tite, A. Chafi, D. Bormann, O. Maksimov, and M. C. Tamargo, J. Appl. Phys. **99**, 063507 (2006).

[35] S. Ghosh, J. B. Neaton, A. H. Antons, M. H. Cohen, and P. L. Leath, Phys. Rev. B **70**, 024206 (2004).

[36] Note that the "no local relaxation" case, corresponding to a regular lattice, reproduces in fact the practice of simulation by Baroni *et al*. (Ref. [9]) in their calculations on Al$_{0.5}$Ga$_{0.5}$As.

[37] G. M. Barrow, J. Chem. Phys. **19**, 345 (1951).

[38] Incidentally, we have extensively discussed in Ref. [6] that the Be-Se stretching ($a.s.$) and Be-Se bending ($r.$, $t.$, $w.$, $sc.$, $s.s.$) of the –Be–Se–Be– impurity motif may be consistently assigned within the percolation scheme, i.e., at one dimension, as the TO$_{\text{Be-Se}}^{\text{Be,1}}$ and TO$_{\text{Be-Se}}^{\text{Zn,1}}$ modes, respectively.